ELSEVIER

Composite Structures 63 (2004) 87–99

COMPOSITE STRUCTURES

www.elsevier.com/locate/compstruct

Design and manufacture of an automotive hybrid aluminum/composite drive shaft

Dai Gil Lee *, Hak Sung Kim, Jong Woon Kim, Jin Kook Kim

Department of Mechanical Engineering, ME3261, Korea Advanced Institute of Science and Technology, 373-1 Guseong-dong, Yuseong-gu, Daejeon-shi 305-701, South Korea

Abstract

Substituting composite structures for conventional metallic structures has many advantages because of higher specific stiffness and higher specific strength of composite materials. In this work, one-piece automotive hybrid aluminum/composite drive shaft was developed with a new manufacturing method, in which a carbon fiber epoxy composite layer was co-cured on the inner surface of an aluminum tube rather than wrapping on the outer surface to prevent the composite layer from being damaged by external impact and absorption of moisture. The optimal stacking sequence of the composite layer was determined considering the thermal residual stresses of interface between the aluminum tube and the composite layer calculated by finite element analysis. Press fitting method for the joining of the aluminum/composite tube and steel yokes was devised to improve reliability and to reduce manufacturing cost, compared to other joining methods such as adhesively bonded, bolted or riveted and welded joints. Protrusion shapes on the inner surface of steel yoke were created to increase the torque capability of the press fitted joint. From experimental results, it was found that the developed one-piece automotive hybrid aluminum/composite drive shaft had 75% mass reduction, 160% increase in torque capability compared with a conventional two-piece steel drive shaft. It also had 9390 rpm of natural frequency which was higher than the design specification of 9200 rpm.

Keywords: Hybrid; One-piece drive shaft; Natural frequency; Press fitting; Protrusion

1. Introduction

An automotive drive shaft transmits power from the engine to the differential gear of a rear wheel drive vehicle as shown in Fig. 1 [1]. The torque capability of the drive shaft for passenger cars should be larger than 3500 Nm and the fundamental bending natural frequency should be higher than 9200 rpm to avoid whirling vibration [2]. Since the fundamental bending natural frequency of a one-piece drive shafts made of steel or aluminum is normally lower than 5700 rpm when the length of the drive shaft is around 1.5 m [2], the steel drive shaft is usually manufactured in two pieces to increase the fundamental bending natural frequency because the bending natural frequency of a shaft is inversely proportional to the square of beam length and proportional to the square root of specific modulus. The two-piece steel drive shaft consists of three universal joints, a center supporting bearing and a bracket, which increases the total weight of an automotive vehicle and decreases fuel efficiency. Since carbon fiber epoxy composite materials have more than four times specific stiffness (E/ρ) of steel or aluminum materials, it is possible to manufacture composite drive shafts in one-piece without whirling vibration over 9200 rpm [3]. The composite drive shaft has many benefits such as reduced weight and less noise and vibration [4]. However, because of the high material cost of carbon fiber epoxy composite materials, rather cheap aluminum materials may be used partly with composite materials such as in a hybrid type of aluminum/composite drive shaft, in which the aluminum has a role to transmit the required torque, while the carbon fiber epoxy composite increases the bending natural frequency above 9200 rpm. However, the hybrid drive shaft requires reliable joining of the hybrid shaft to steel or aluminum yoke of a universal joint, which is often the most difficult task [1,2].

Generally, there are three kinds of joining methods: adhesive joining, welding and mechanical joining with bolts or rivets. The adhesively bonded joint uses an

* Corresponding author. Tel.: +82-42-869-3221; fax: +82-42-869-5221.

E-mail address: dglee@kaist.ac.kr (D.G. Lee).

0263-8223/$ - see front matter © 2003 Published by Elsevier Ltd.
doi:10.1016/S0263-8223(03)00136-3

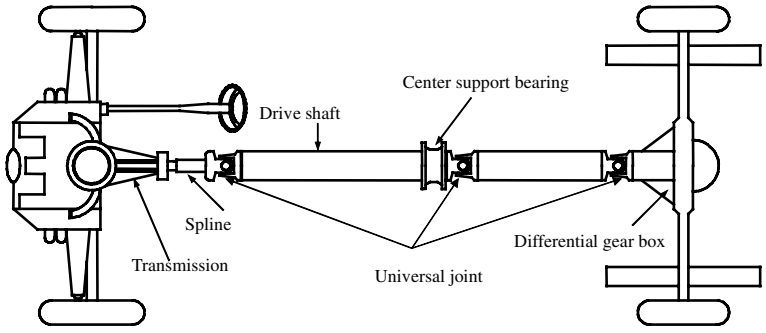

Fig. 1. Schematic diagram of the conventional two-piece steel drive shaft for a rear wheel driving vehicle.

adhesive interlayer between adherends. The adhesively bonded joint can distribute the required load over a larger area than the mechanical joint, requires no holes, adds very little weight to structures and has superior fatigue resistance. However, the adhesively bonded joint requires the careful surface preparation of the adherend, is affected by service environments and is difficult to disassemble for inspection and repair [5,6]. The welding is created by the coalescence of two metal substrates, which is achieved by a combination of temperature, pressure, and metallurgical condition. During welding, the inner composite materials of the hybrid drive shaft may be degraded due to temperature rise of outer metal materials [7]. The mechanical joint is created by fastening the substrates with bolts or rivets. Since it requires holes for bolts and rivets, stress concentration, fatigue and galvanic corrosion problems are vulnerable to occur at the holes.

Many researchers have investigated hybrid drive shafts and joining methods of the hybrid shafts to the yokes of universal joints. The first composite drive shaft was developed by the Spicer U-Joint Division of Dana Corporation for the Ford econoline van models in 1985. The general motors pickup trucks which adopted the Spicer product enjoyed a demand three times that of projected sales in its first year (1988) [8]. Cho et al. [9] developed a compressive preloading method to reduce the thermal residual stress of a hybrid aluminum/composite shaft in the axial direction during curing operation, which increased the fatigue characteristics of the hybrid aluminum/composite shaft. Kim et al. [4] designed a hybrid composite drive shaft, which was composed of high stiffness carbon fiber epoxy and glass fiber epoxy composites, and investigated the optimal design of adhesively bonded joints for the composite drive shaft with respect to bond thickness, bond length and yoke thickness.

In most studies of hybrid composite drive shafts, a composite layer was stacked on the outer surface of a metal tube for easy manufacturing. However, the outside composite layer may be damaged or delaminated by external low velocity impacts or degraded by water absorption into the composite outside layer [10,11]. Therefore, in this paper, an one-piece automotive hybrid aluminum/composite drive shaft was developed with a new manufacturing method, in which the carbon fiber epoxy composite layer was stacked and co-cured on the inner surface of the aluminum tube, which eliminates the possibility of the damage of the composite layer as well as the moisture absorption as depicted in Fig. 2. The optimal stacking sequence of the composite layers was determined considering thermal residual stresses and the failure index of interface between the aluminum tube and the composite layer calculated by finite element analysis. Press fitting method for fastening the aluminum/composite shaft and steel yokes was employed to

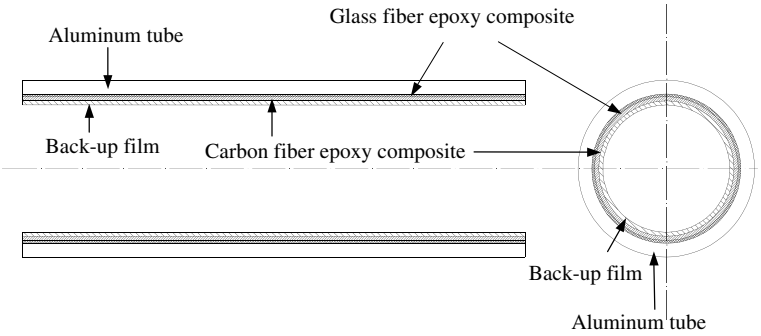

Fig. 2. Schematic diagram of the co-cured aluminum/composite drive shaft.

improve reliability and to reduce manufacturing cost, rather than other joining methods such as adhesive joint, mechanical joint and welding. Optimal protrusion shape for the inner surface of the steel yoke was designed to increase the torque capability of the press fitted joint from the finite element analysis and the torque capability of the press fitted joint was compared with the experimental result. Finally, the one-piece automotive hybrid aluminum/composite drive shaft was manufactured and its static torque transmission capability and fundamental vibration frequency were measured.

2. Design of the aluminum/composite drive shaft

The aluminum/composite drive shaft should satisfy three design specifications such as static torque capability, buckling torque capability and bending natural frequency. The major role of the aluminum tube is to sustain an applied torque while the role of the carbon fiber epoxy composite is to increase bending natural frequency. The carbon fiber epoxy prepreg was USN150 manufactured by SK Chemicals (Korea), whose properties are similar to T300/5208. Tables 1 and 2 show the mechanical properties of the carbon fiber epoxy composite and the aluminum tube (6061-T6), respectively.

The torque transmitted by the hybrid drive shaft, T is the sum of the torque transmitted by the aluminum tube, T_{al} and that by the composite layer, T_{co} [3,12]:

$$T = T_{al} + T_{co} \tag{1}$$

Considering geometric compatibility and material properties of each material, the torque transmitted by the aluminum tube is calculated as follows:

Table 2
Mechanical properties of the aluminum (6061-T6) and the steel (SM45C)

Mechanical properties	Aluminum	Steel
Tensile modulus, E (GPa)	72.0	207.0
Shear modulus, G (GPa)	27.0	80.0
Poisson's ratio, v	0.33	0.3
Density, ρ (kg/m^3)	2700	7600
Yield strength, S_Y (MPa)	270	370
Shear strength, S_S (MPa)	200	–

$$T_{al} = \frac{G_{al} \cdot J_{al}}{G_{al} \cdot J_{al} + G_{co} \cdot J_{co}} T \tag{2}$$

where G is shear modulus, J is the polar moment of inertia, and subscripts 'al' and 'co' represent the aluminum tube and the composite layer, respectively. The shear modulus G_{al} and the polar moment of inertia of the aluminum tube J_{al} are much larger than those of the composite layer because only thin layer of unidirectional composite can increase sufficiently the natural frequency of the hybrid drive shaft. Therefore, the torque transmitted by the aluminum tube only is almost same as the torque transmitted by the hybrid aluminum/composite shaft. From now on, the static and buckling torque capabilities of the aluminum/composite shaft will be calculated neglecting the composite layer as follows [12]:

$$T_{static} = 2\pi \cdot r_{ave}^2 \cdot t_{al} \cdot S_{S,al} \tag{3}$$

$$T_{buckling} = \frac{\pi\sqrt{2} \cdot E_{al}}{3(1 - v_{al}^2)^{0.75}} \sqrt{(r_{ave} \cdot t_{al}^5)} \tag{4}$$

where T_{static} and $T_{buckling}$ are the static and buckling torque capabilities of the hybrid aluminum/composite shaft, respectively, and r_{ave} is the average radius of the aluminum tube, t_{al} is the thickness of the aluminum

Table 1
Mechanical properties of the composite materials

Material	Unidirectional carbon fiber epoxy composite (USN150)	Unidirectional glass fiber epoxy composite (UGN150)	Crowfoot satin woven glass fiber epoxy (GEP215)
E_1 (GPa)	131.6	43.3	35.5
E_2, E_3 (GPa)	8.20	14.7	17.2
G_{23} (GPa)	3.5	3.5	3.5
G_{12}, G_{13} (GPa)	4.5	4.4	3.7
v_{12}, v_{13}	0.281	0.3	0.22
α_1 ($\times 10^{-6}$/°C)	−0.9	6.3	8.3
α_2, α_3 ($\times 10^{-6}$/°C)	27	19	12.2
S_1^t (MPa)	2000	1050	600
S_1^c (MPa)	−1400	700	700
S_2^t, S_3^t (MPa)	61	65	100
S_2^c, S_3^c (MPa)	−130	−120	−120
S_{23} (MPa)	40	65	60
S_{13}, S_{12} (MPa)	70	40	40
ρ (kg/m^3)	1550	2100	2050
t_{ply} (mm)	0.125	0.12	0.15

E_1: Longitudinal modulus; E_2, E_3: transverse modulus; G_{12}, G_{13}: 12-direction, 13-direction shear modulus; G_{23}: 23-direction shear modulus; v_{12}: 12-direction poisson's ratio; v_{13}: 13-direction poisson's ratio; α_1: longitudinal CTE; α_2, α_3: transverse CTE; S_1^t: longitudinal tensile strength; S_1^c: longitudinal compressive strength; S_2^t, S_3^t: transverse tensile strength; S_2^c, S_3^c: transverse compressive strength; S_{12}, S_{13}: 12-direction, 13-direction shear strength; S_{23}: 23-direction shear strength; ρ: density; t_{ply}: thickness of composite.

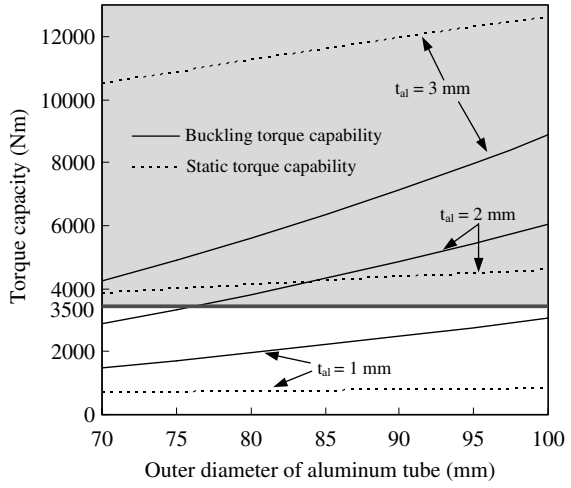

Fig. 3. Torque capability of the aluminum tube with respect to the outer diameter and thickness (t_{al}) of the aluminum tube calculated from Eqs. (3) and (4) (Design torque $\geqslant$ 3500 Nm).

tube, $S_{S,al}$ is the shear strength of the aluminum, E_{al} is the elastic modulus of aluminum, and v_{al} is the poisson's ratio of aluminum. The static and buckling torque capabilities of the aluminum/composite shaft are shown in Fig. 3 with respect to the outer diameter $(2 \cdot r_{ave} + t_{al})$ and thickness (t_{al}) of the aluminum tube. Since the outer diameter of the drive shaft is normally limited to 100 mm for passenger cars, the outer diameter and thickness of the aluminum tube were determined to be 90 mm and 2 mm, respectively.

The fundamental bending natural frequency of drive shafts f_n was calculated by the following equation with the simply supported boundary condition on the both ends [13].

$$f_n = \frac{9.869}{L^2}\sqrt{\frac{E_{al}I_{al} + E_{co}I_{co}}{\rho_{al} + \rho_{co}}} \tag{5}$$

where E is the elastic modulus in the axial direction of drive shaft, I is the sectional moment of inertia, ρ is the mass per unit length, and L is the length of the drive shaft. The aluminum/composite shaft was composed of the aluminum tube, the glass fiber epoxy composite, the carbon fiber epoxy composite, and the back-up film from outside as shown in Fig. 2. The glass fiber epoxy prepreg was firstly laid-up on the inner surface of the aluminum tube for an insulating material to eliminate galvanic corrosion between the aluminum and carbon fiber epoxy composite. Either a unidirectional glass fiber epoxy prepreg (UGN150, SK Chemicals, Korea) or a crowfoot satin woven glass fiber epoxy prepreg (GEP215, SK Chemicals, Korea), whose warp and weft ratio was 7–3, was selected as the insulating material depending on the stress distribution. The mechanical properties of the glass fiber epoxy composites are shown in Table 1. The stacking angle of the carbon fiber epoxy

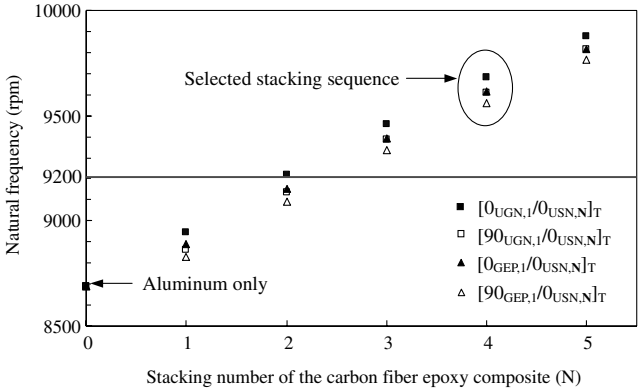

Fig. 4. Bending natural frequency of the aluminum/composite drive shaft with respect to the number of stacked plies of carbon fiber epoxy prepregs (ply thickness = 0.125 mm), and the type and stacking angle of the insulating materials (Design specification $\geqslant$ 9200 rpm).

composites was chosen to be 0° from the shaft axis to maximize the elastic modulus in the axial direction. The bending natural frequency of the aluminum/composite drive shaft was calculated with respect to the stacking number of the carbon fiber epoxy prepregs and the stacking sequence of the glass fiber epoxy composites, when the length of the aluminum/composite drive shaft was 1.32 m. As shown in Fig. 4, the bending natural frequency of the aluminum/composite drive shaft increased in accordance with the amount of the carbon fiber epoxy composite. When more than three plies of carbon fiber epoxy prepregs are used, the natural frequency of the aluminum/composite drive shaft is higher than 9200 rpm, regardless of the stacking sequence of the glass fiber epoxy composites. Therefore, in this work, four plies (0.5 mm) of the carbon fiber epoxy prepregs were used for the safety margin of the drive shaft.

3. Selection of the glass fiber epoxy composite as an insulating material

The stacking sequence of the insulating glass fiber epoxy composites was determined considering the thermal residual stress and the failure index of the composite layer under the applied torque. In order to determine the optimum stacking sequence of the insulating glass fiber epoxy composites, the thermal residual stress was calculated with respect to the stacking angle and the insulating material type of the glass fiber epoxy composites by finite element analysis using ABAQUS 6.2 (Hibbitt, Karlsson & Sorensen, USA), a commercial software. The aluminum/composite shaft was modeled using the four-node two-dimensional axi-symmetry elements (CGAX4) as shown in Fig. 5. Total number of the nodes and elements were 7010 and 6300, respectively. The outer diameter and thickness of the aluminum tube were

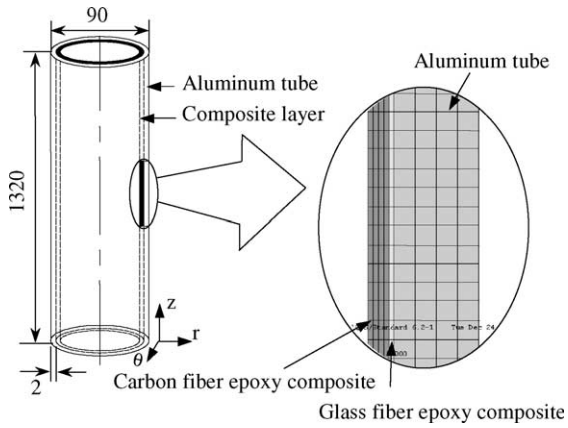

Fig. 5. Finite element model of the aluminum/composite drive shaft (units in mm).

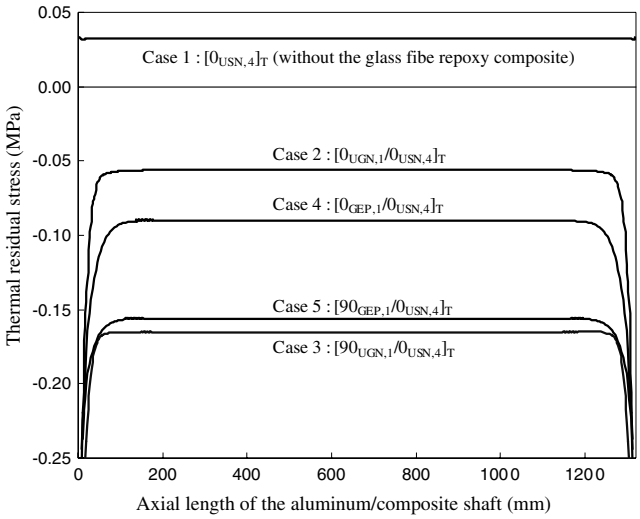

Fig. 6. Interlaminar tensile thermal residual stress distributions in the composite layer in the thickness direction versus the axial length of the aluminum/composite shaft.

90 and 2 mm, respectively. Since bonding thickness between the aluminum tube and the composite layer was very small (5–10 μm) when co-cured under the pressure of 0.6 MPa [14], perfect bonding between the aluminum tube and composite layers was assumed for the finite element analysis. A compressive preloading procedure for eliminating the thermal residual stress in the aluminum tube in the axial direction was included in the analysis step. The thermal residual stress of the aluminum tube in the axial direction was eliminated at room temperature by giving an axial compressive preload −170 MPa on the aluminum tube because it improved the fatigue characteristics of the co-cured aluminum/composite shaft [9]. Five stacking sequences were considered in the analysis as listed in Table 3. The carbon fiber epoxy prepregs were stacked in the axial direction for all the cases, while the stacking angle of glass fiber epoxy prepreg was varied. For the stacking sequence of Case 1, only carbon fiber epoxy composite layers were stacked on the inside surface of the aluminum tube without the glass fiber epoxy composite. For the stacking sequences of Cases 2 and 3, unidirectional glass fiber epoxy prepregs were stacked axially or transversely. For the stacking sequences of Cases 4 and 5, crowfoot satin woven glass fiber epoxy prepregs were stacked first, followed by the stacking of carbon fiber epoxy composite layer. The stacking angles of crowfoot satin woven glass fiber epoxy prepregs for each case were 0° and 90°, respectively. Fig. 6 shows the interlaminar tensile thermal residual stresses σ_r in the composite layer adjacent to the aluminum tube with respect to the stacking sequence. For the Case 1, a tensile peel stress occurred because the coefficient of thermal expansion (CTE) of the carbon fiber epoxy composite in the circumferential direction (27.0×10^{-6}/°C) was larger than that of the aluminum tube (23.6×10^{-6}/°C), which might induce a delamination between the aluminum tube and the composite layer [15]. However, a compressive interlaminar stresses in the thickness direction occurred in all other cases because the CTE of the glass fiber epoxy composites in the circumferential direction were smaller than that of the aluminum tube, which may improve the fatigue strength of the hybrid composite shaft [15].

Table 3
Stacking sequence of the glass fiber epoxy composite and the carbon fiber epoxy composite layer stacked on the inner surface of the aluminum tube

Case number	Stacking sequence from the inner surface of the aluminum tube
1	$[0_{USN,4}]_T$ (without the glass fiber epoxy composite)
2	$[0_{UGN,1}/0_{USN,4}]_T$
3	$[90_{UGN,1}/0_{USN,4}]_T$
4	$[0_{GEP,1}/0_{USN,4}]_T$
5	$[90_{GEP,1}/0_{USN,4}]_T$

The stresses in the composite layer were also calculated with respect to the stacking sequence when a maximum buckling torque of 4360 Nm of aluminum tube was applied to the aluminum/composite shaft. The stress distributions in the composite layer adjacent to the aluminum tube with respect to the stacking sequence are shown in Fig. 7. In order to assess the failure index of the composite layer under the applied torque with respect to the stacking sequence, the following Tsai–Wu failure index of the composite layer was calculated [16].

$$FI = F_1\sigma_1 + F_2\sigma_2 + F_3\sigma_3 + F_{11}\sigma_1^2 + F_{22}\sigma_2^2 + F_{33}\sigma_3^2 + F_{44}\sigma_4^2 + F_{55}\sigma_5^2 + F_{66}\sigma_6^2 + 2F_{12}\sigma_1\sigma_2 + 2F_{13}\sigma_1\sigma_3 + 2F_{23}\sigma_2\sigma_3 \quad (6)$$

where

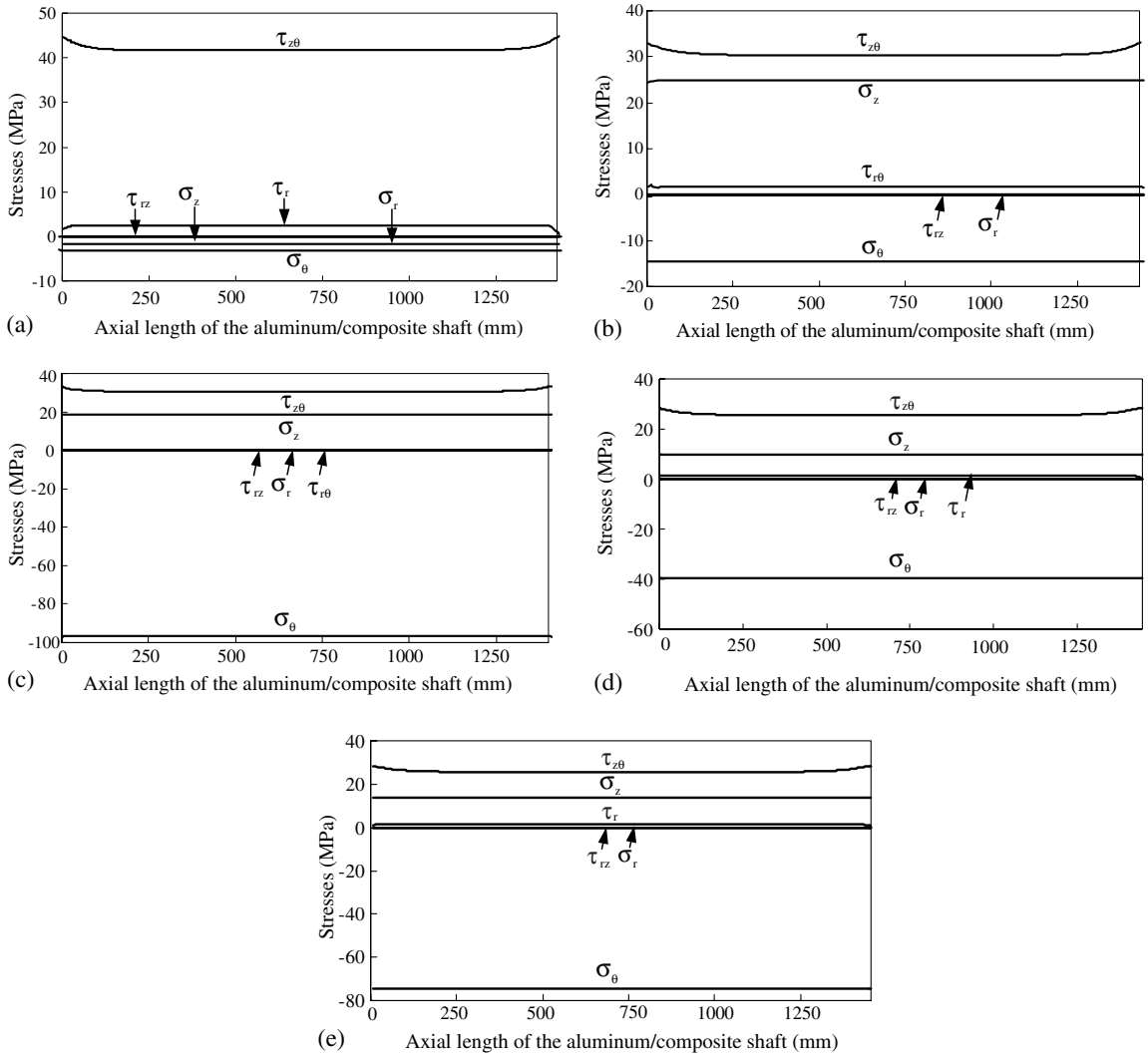

Fig. 7. Stress distributions in the composite layer adjacent to the aluminum tube when a torque of 4360 Nm was applied to the aluminum/composite shaft: (a) Case 1, $[0_{USN,4}]_T$; (b) Case 2, $[0_{UGN,1}/0_{USN,4}]_T$; (c) Case 3, $[90_{UGN,1}/0_{USN,4}]_T$; (d) Case 4, $[0_{GEP,1}/0_{USN,4}]_T$; (e) Case 5, $[90_{GEP,1}/0_{USN,4}]_T$.

$$
\begin{aligned}
&F_1 = \frac{1}{S_1^t} + \frac{1}{S_1^c}, \quad F_2 = \frac{1}{S_2^t} + \frac{1}{S_2^c}, \quad F_3 = \frac{1}{S_3^t} + \frac{1}{S_3^c},\\
&F_{11} = -\frac{1}{S_1^t S_1^c}, \quad F_{22} = -\frac{1}{S_2^t S_2^c}, \quad F_{33} = -\frac{1}{S_3^t S_3^c},\\
&F_{44} = \frac{1}{S_{23}^2}, \quad F_{55} = \frac{1}{S_{13}^2}, \quad F_{66} = \frac{1}{S_{12}^2},\\
&F_{12} = -\frac{\sqrt{F_{11}F_{22}}}{2}, \quad F_{23} = -\frac{\sqrt{F_{22}F_{33}}}{2}, \quad F_{13} = -\frac{\sqrt{F_{11}F_{33}}}{2}
\end{aligned}
\tag{7}
$$

Fig. 8 shows the failure index of the composite layer adjacent to the aluminum tube with respect to the stacking sequence when a torque of 4360 Nm was applied. The failure index of the carbon fiber epoxy composite layers was 0.38 in all cases, while the failure index in the glass fiber epoxy layer were higher than this value. The failure index in the glass fiber epoxy layer of the Case 3 had the highest failure index of 0.95. The Case 1 had the lowest failure index of 0.38 and the Case 5 had the value of 0.55.

Therefore, the stacking sequence of the Case 5, in which crowfoot satin woven glass fiber epoxy prepreg was stacked transversely (90°) between the carbon fiber epoxy composite layer and the aluminum tube, was selected because the compressive thermal residual peel stress in the thickness direction was relatively high compared to those of other cases and the failure index by the applied torque was lower than other cases except the Case 1.

4. Press fitted joint with protrusions

The press fit joining method between the hybrid aluminum/composite shaft and the steel yokes with protrusions was developed to increase reliability and to

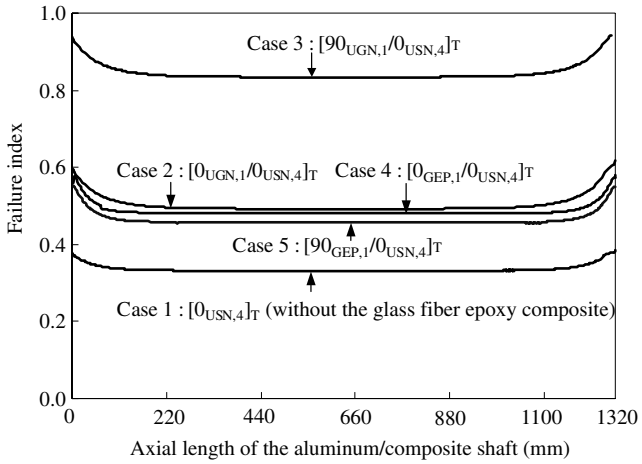

Fig. 8. Failure indices of the composite layer adjacent to the aluminum tube with respect to the stacking sequence of the composite layer when a torque of 4360 Nm was applied to the aluminum/composite shaft.

reduce manufacturing cost compared to other joining methods. To improve the torque capability of the press fitted joint, the protrusions in the axial direction were generated on the inner surface of the steel yoke as shown in Fig. 9. The protrusions on the inner surface of the steel yoke could engrave grooves on the surface of the aluminum shaft during press fitting process, which made mechanical interlocking between the steel protrusions and the engraved grooves on the surface of the aluminum tube. The protrusions on the inner surface of the steel yoke would be easily formed by broaching or die pressing in mass production, however, in this work an electro discharge machining (EDM) method was used for the prototype manufacturing. The joining between the aluminum tube and the steel yoke was secured more by the press fitting operation, which might reduce

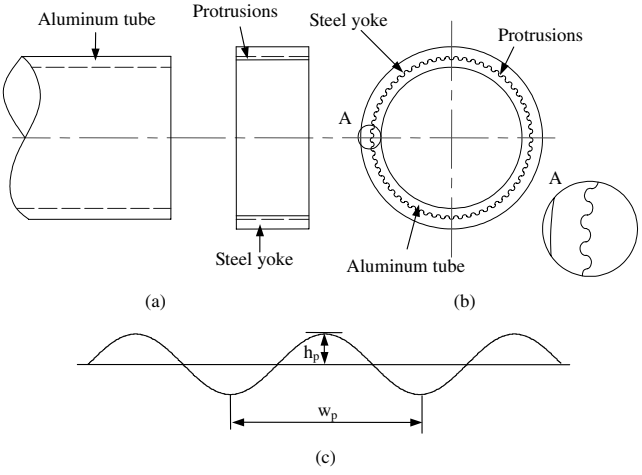

Fig. 9. Schematic diagram of press fitted joining method: (a) disassembled parts; (b) after assembly; (c) sinusoidal shape protrusion with aspect ratio h_p/w_p.

manufacturing time and cost eliminating several joining processes. Since the fatigue characteristics of the press fitted joint with protrusions would be affected by the protrusion shape, the optimal protrusion shape was sought.

Fatigue failures of the press fitted joint with protrusions would occur by two reasons: the stress concentration in the protrusions, and the fretting fatigue when torque applied. If the protrusions had sharp edges, the stress concentration would become high, which decreases the fatigue strength. Therefore, the protrusion shape should be smooth enough to reduce stress concentration. The fretting fatigue of contacting surface between the steel protrusions and the grooves on the surface of aluminum tube may be eliminated by giving a compressive stress between the mating surfaces, which prevents the relative motion [17]. The fretting accelerates fatigue crack growth in mechanical components of engineering structures, which causes considerable reduction of the fatigue strength of a press-fitted assembly. It has been known that the fretting fatigue strength reduces much when the amplitude of the slip is higher than 50 μm [18]. Therefore, the slip amplitude between the steel protrusions and the grooves on the surface of the aluminum tube of the press fitted joint by applied torque should be reduced.

To reduce the stress concentration in the protrusions, a sinusoidal shape protrusion was selected because of its smoothness and easy representation. In the sinusoidal protrusions shape as shown in Fig. 9(c), h_p and w_p represent the height and width of the sinusoidal protrusions, respectively. The slip amplitude of contact surfaces between the protrusions of the steel yoke and the generated grooves on the surface of the aluminum tube under a given magnitude of torque was calculated by finite element analysis using ABAQUS 6.2. Fig. 10 shows the finite element model of the press fitted joint between the aluminum tube and the steel yoke, which are interlocked by the sinusoidal shape protrusions. Since the finite element model for the stress state and the slip distance of the press fitted joint was axi-symmetric, only 1/180 (3°) portion of the press fitted joint was modeled using the eight-node three-dimensional solid elements (C3D8R). The material properties of the aluminum tube (6061-T6) and the steel yoke (SM45C) are listed in Table 3. Idealized elastic-perfectly plastic properties for the steel yoke and the aluminum tube were used based on the yield strengths as shown in Fig. 11. The friction coefficient of 0.31 between the aluminum and the steel was used. The press fitted length of 10 mm was used in the analysis to save computing time although the actual fitting length was larger than this value. The slip amplitude between the aluminum and the steel protrusions was calculated with respect to the height and the width of the sinusoidal protrusions when a torque 4360 Nm was applied to the steel yoke, which

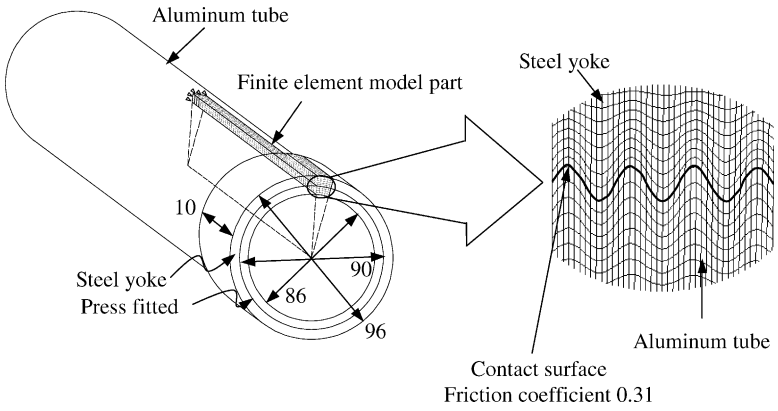

Fig. 10. Finite element model of the press fitted joint with eight-node three-dimensional solid elements for the contact slip analysis (units in mm).

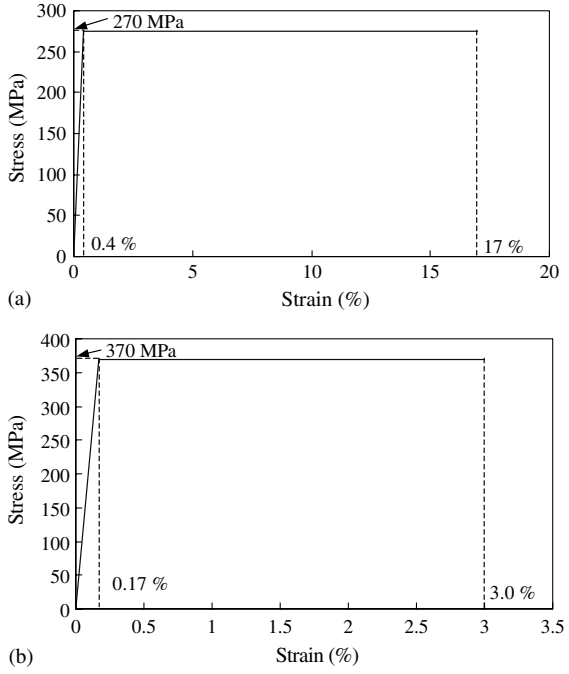

Fig. 11. Idealized elastic-perfectly plastic stress–strain curves for the aluminum tube and the steel yoke: (a) aluminum (6061-T6); (b) steel (SM45C).

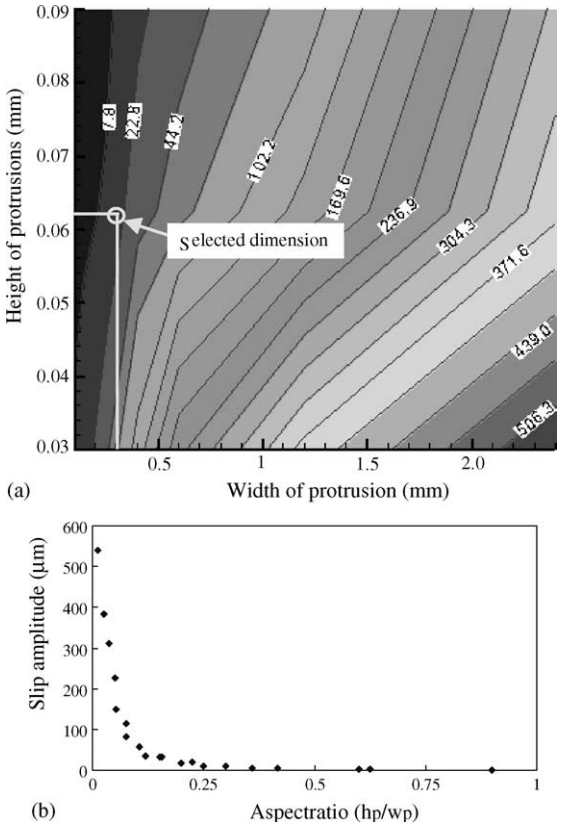

Fig. 12. Slip amplitude (μm) of protrusions: (a) with respect to the height and width of sinusoidal protrusions; (b) with respect to the aspect ratio (h_p/w_p) of protrusions.

was the buckling torque capability of the aluminum tube. Fig. 12(a) shows the slip amplitude with respect to the height and width of the sinusoidal protrusions. The slip amplitude decreased as the aspect ratio of the sinusoidal protrusions (h_p/w_p) increased regardless of the width and the height of protrusions as shown in Fig. 12(b), which was reproduced from the results of Fig. 12(a). The slip amplitude was smaller than 10 μm, when the aspect ratio of sinusoidal protrusions was larger than 0.25. The stress concentration increased as the aspect ratio of the protrusions increased [19]. Therefore, in order to minimize the stress concentration under the constraint of the slip, the aspect ratio of 0.25 for the sinusoidal protrusion was selected.

As the height of the protrusions increases, the press force for the press fitting operation increases, which may fail the aluminum/composite drive shaft during the press fitting operation with the steel yokes. Therefore, the width of protrusions of 0.25 mm was selected because the smaller width of protrusion than this value was difficult to be machined by EDM cutting. Then, the height of protrusions was 0.0625 mm. Fig. 13 shows the stress distributions in the protrusions of the aluminum

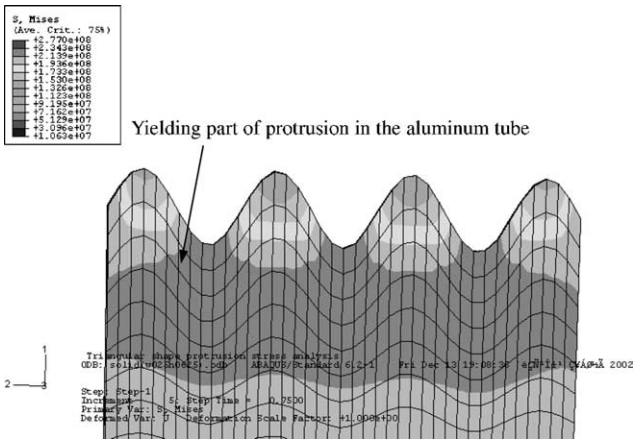

Fig. 13. Stress distributions in the protrusions of the aluminum tube when a torque of 4360 Nm was applied to the press fitted joint whose press fitted length was 10 mm when w_p and h_p of the protrusions were 0.25 and 0.0625 mm, respectively.

tube under the applied torque of 4360 Nm torque, in which the whole sections of the protrusions in the aluminum tube were yielded. Under the assumption that the press fitted joint would fail when the stress in whole section of the protrusions in the aluminum tube reached

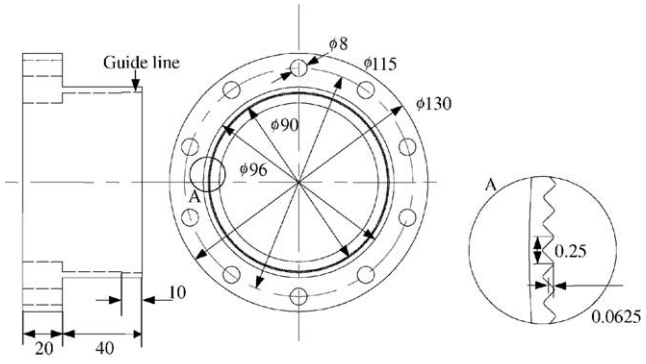

(a)

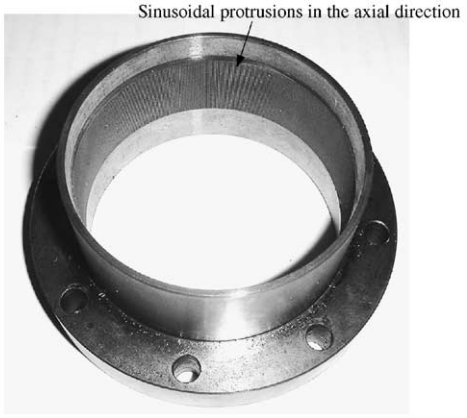

(b)

Fig. 14. Steel yoke specimen for the press fitted joint: (a) drawings (dimensions in mm); (b) photograph.

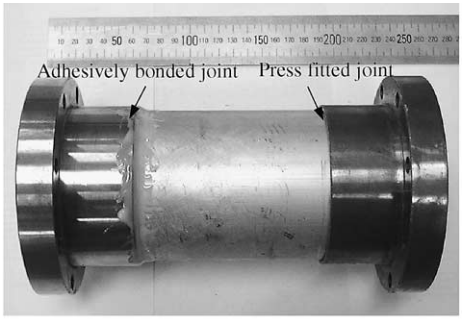

(a)

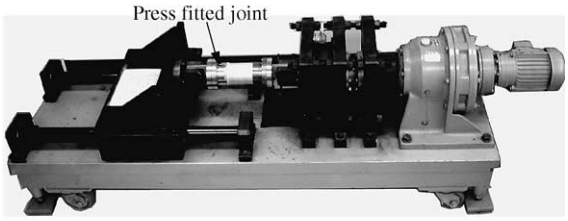

(b)

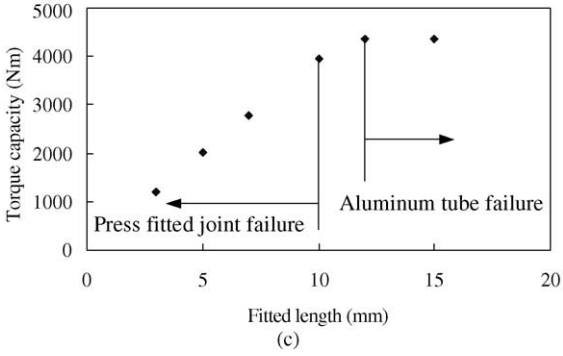

(c)

Fig. 15. Press fitted joint for torque tests: (a) specimen; (b) torque tester; (c) torque capability of the press fitted joint with respect to fitted length.

the yield strength, the torque capability of the press fitted joint was 4360 Nm. The average shear strength τ of the press fitted joint was defined in this work as follows:

$$\tau = \frac{T}{2\pi r^2 L} \tag{8}$$

where T, r and L represent the torque capability, radius and fitted length of the press fitted joint, respectively. From Eq. (8), the average shear strength of the press fitted joints with protrusions was 34 MPa, which was 1.5

Table 4
Specification of the torque tester

Maximum torque (Nm)	13,000
Stroke (mm)	600
Maximum length of a specimen (mm)	520
Speed of testing (°/s)	0.02–0.7
Encoder resolution (°)	0.088

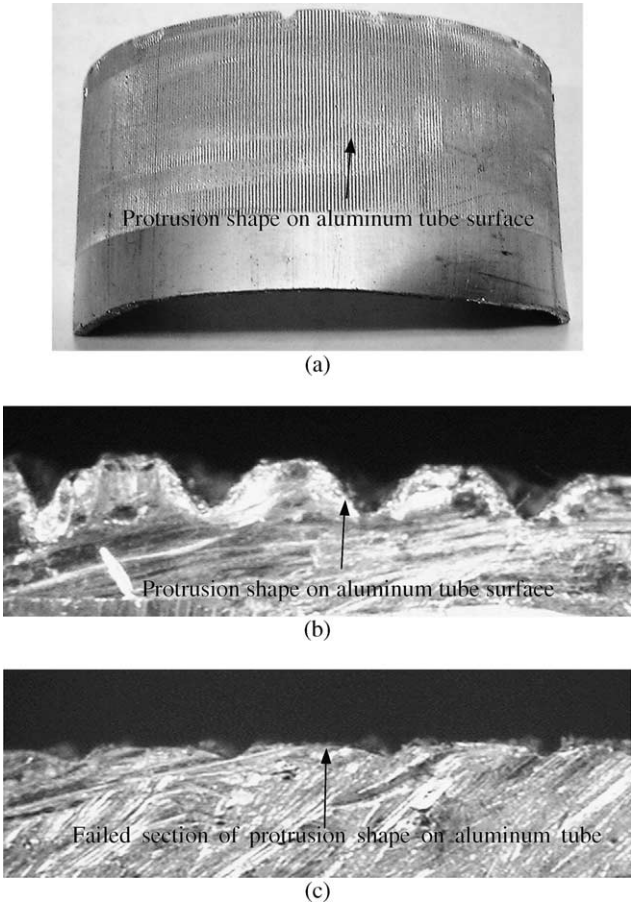

Fig. 16. Microscopic view of surface of the aluminum tube after disassembling from the press fitted joint (×100): (a) surface of the aluminum tube; (b) section view of the aluminum tube before failure of press fitted joint; (c) section view of the aluminum tube after failure of press fitted joint.

times higher than that of the adhesively bonded joint obtained from the experimental results of Kim et al. [4].

To investigate the torque capability of the press fitted joint with the protrusions, the steel yoke whose inner surface had the protrusions in the axial direction was manufactured as shown in Fig. 14. The protrusions were machined by EDM wire cutting method and the shape of the protrusion was sinusoidal whose height and width were 0.0625 and 0.25 mm, respectively, same as the designed values. The outer and inner diameters of the aluminum tube were 90 and 86 mm, respectively. The one end of the aluminum tube and the steel yoke were fitted using press fitting operation and the other end of the aluminum tube was adhesively bonded to the jig for the torque test as shown in Fig. 15(a). Static torque test of the press fitted joint was performed with respect to the fitted length using the torque tester as shown in Fig. 15(b). Table 4 shows the specification of the torque tester. Fig. 15(c) shows the torque capability of the press fitted joint with respect to the fitted length. Buckling failure of the aluminum tube occurred above 12 mm fitted length. The torque capability of the press fitted joint was linearly proportional to the fitted length up to 10 mm. The average shear strength of the press fitted joint was about 30 MPa regardless of the fitted length, which was about 88% of the calculated result. The difference between the experimental result and the calculated result might be due to the irregular interlocking between the protrusions of the steel yoke and the aluminum tube.

The surface of the aluminum tube was observed using a microscope after disassembling the aluminum tube from the press fitted joint. Fig. 16(a) and (b) show that the grooves on the surface of the aluminum tube was engraved by the steel protrusions during the press fitting process. Fig. 16(c) shows that the failed protrusions engraved on the surface of the aluminum tube by the steel yoke. It was similar to the failure mode predicted from the finite element analysis. The torque capability of the press fitted joint between the aluminum tube and the steel yoke was estimated to be 4360 Nm if there was no buckling failure of the aluminum tube, calculated from the average shear strength of 30 MPa when the fitted length was 12 mm.

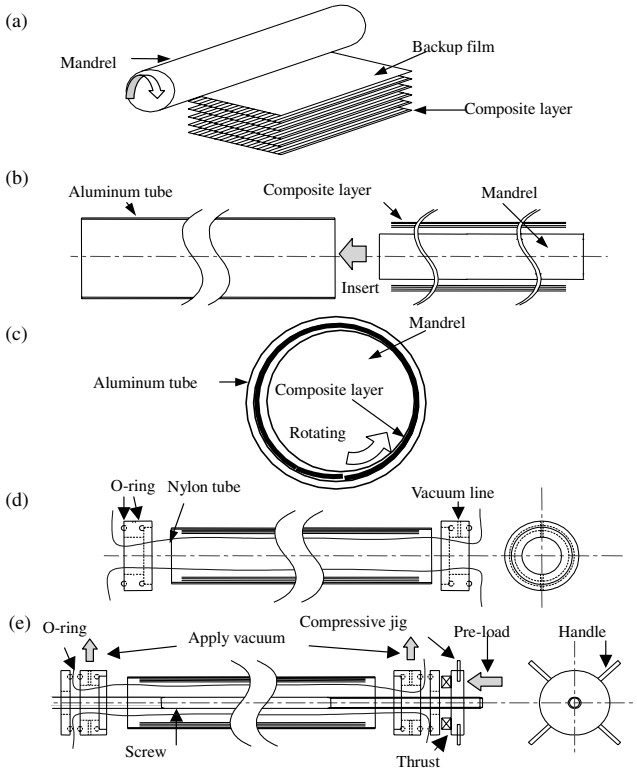

Fig. 17. Manufacturing procedure for the aluminum/composite drive shaft: (a) stacking four carbon fiber epoxy composite layers and one glass fiber epoxy composite layer on a mandrel; (b) inserting the mandrel with the wrapped composite layer into the aluminum tube; (c) stacking the composite layer using mandrel on the inner surface of the aluminum tube; (d) inserting a vacuum bag and fixing caps which have a vacuum line and O-rings; (e) applying preload and curing.

5. Manufacturing

Aluminum/composite hybrid shaft was manufactured using the following processes as depicted in Fig. 17.

(a) Stacking four carbon fiber epoxy composite layers and one glass fiber epoxy composite layer on a mandrel.
(b) Inserting the mandrel with the wrapped composite layers into the aluminum tube.
(c) Stacking the composite layers rotating the mandrel with pressure on the inner surface of the aluminum tube.
(d) Inserting a vacuum bag and fixing caps which have a vacuum line and O-rings.
(e) Applying the preload and curing by the autoclave vacuum bag degassing molding method.

Fig. 18(a) and (b) shows the inner surface of the manufactured aluminum/composite shaft and the steel yoke whose inner surface has the sinusoidal protrusions in the axial direction. After manufacturing the co-cured aluminum/composite hybrid shaft, the steel yoke with the sinusoidal protrusions was press-fitted to the aluminum/composite hybrid shaft. The fitted length of the press fitted joint was 12 mm which was expected to have 4360 Nm torque capability. Fig. 18(c) shows the manufactured one-piece aluminum/composite drive shaft and the conventional two-piece steel drive shaft. The mass of the aluminum/composite drive shaft was 3.3 kg which was only 25% of that of the conventional two-piece steel drive shaft.

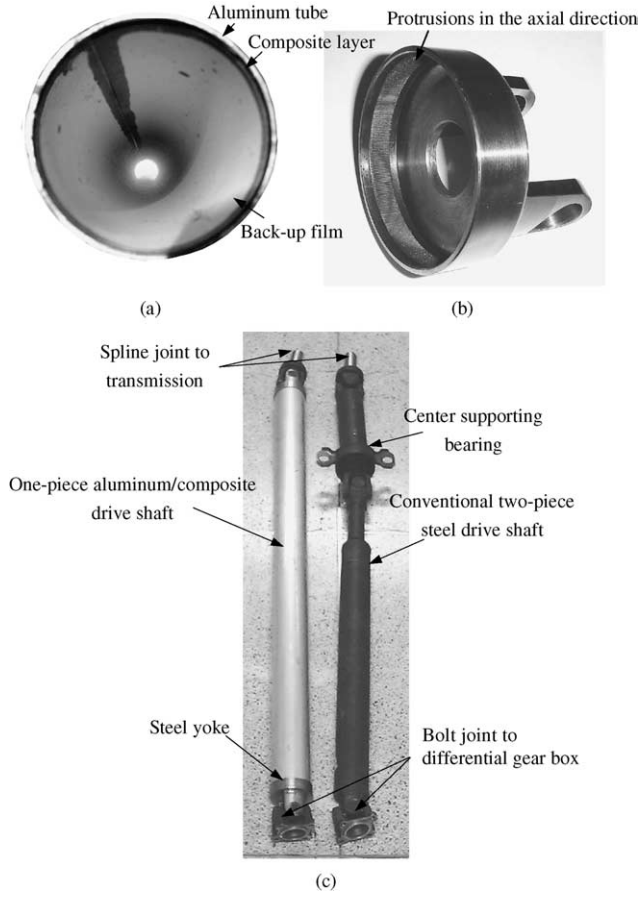

Fig. 18. Photographs of the parts of drive shaft: (a) the inner surface of the manufactured aluminum/composite shaft; (b) the steel yoke with protrusions in the axial direction on the inner surface for drive shaft; (c) prototype of the aluminum/composite drive shaft and the conventional two-piece steel drive shaft.

6. Performance of the aluminum/composite drive shaft

The static torque capability of the aluminum/composite drive shaft was measured using the specimen of 250 mm length, which was a shortened specimen to be mounted on the torque tester. Fig. 19(a) shows the torque-distorsion angle diagram of the shaft with the maximum torque of 4320 Nm. The shaft was buckled at the maximum torque of 4320 Nm as shown in Fig. 19(b). The delamination failure of the composites and the failure of protrusions on the press fitted joint were not found until the aluminum tube was buckled. The torque capability of the aluminum/composite drive shaft of 4320 Nm was slightly higher than the design value.

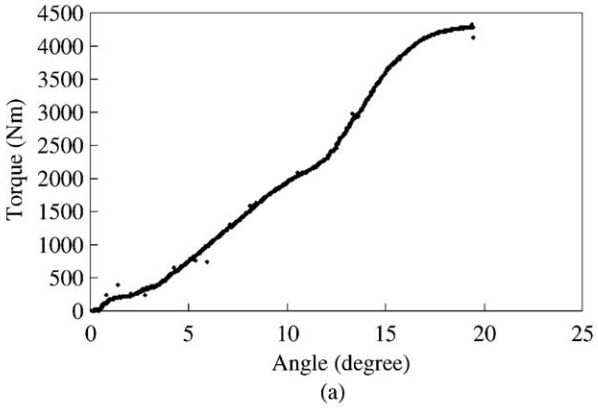

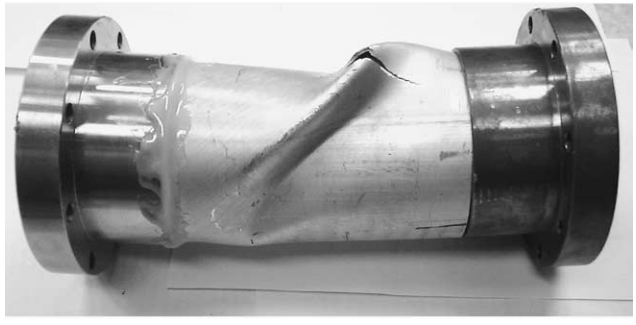

(b)

Fig. 19. Static torque test results of the aluminum/composite drive shaft: (a) torque-distortion angle diagram; (b) buckled specimen after the static torque test.

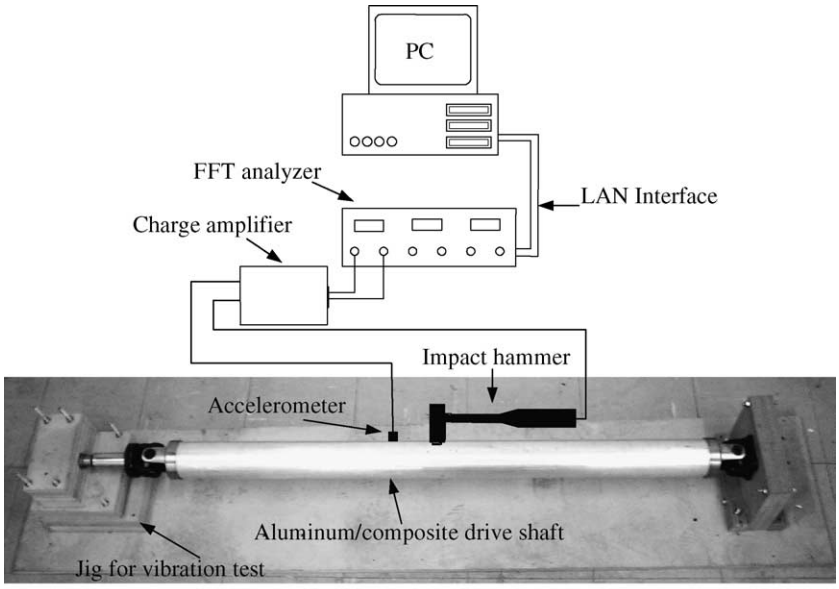

(a)

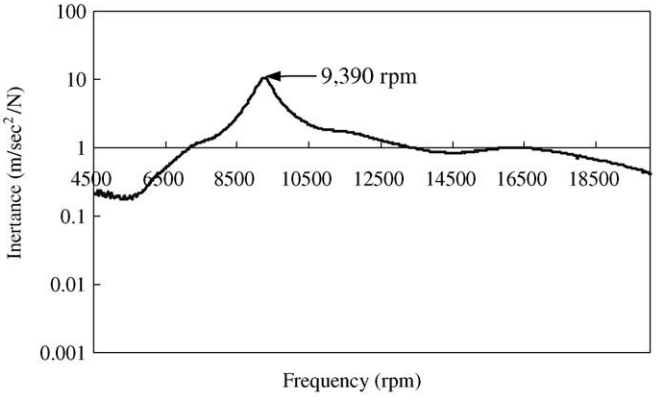

(b)

Fig. 20. Vibration test results of the aluminum/composite drive shaft: (a) vibration test setup; (b) frequency response results.

The vibration test was also performed to investigate the fundamental bending natural frequency of the aluminum/composite drive shaft. In order to simulate the operational condition, a vibration test jig was used for the vibration test of the aluminum/composite drive shaft as shown in Fig. 20(a). The fundamental bending natural frequency of the aluminum/composite drive shaft was 9390 rpm which was also above the design specification of 9200 rpm as shown in Fig. 20(b).

7. Conclusion

In this paper, a one-piece hybrid aluminum/composite drive shaft for a rear wheel drive automobile was developed with a new manufacturing method. The composite materials were stacked on the inner surface of the aluminum tube and co-cured to prevent the hybrid shaft from being damaged by external impact and moisture. The optimal stacking sequence for the composite stacked on the inner surface of the aluminum tube was determined considering the thermal residual stress induced during co-curing operation. A press fit joining method between the steel yoke with protrusions on its surface and the aluminum tube was developed to increase the reliability of joining and to reduce manufacturing cost. The mass of the manufactured hybrid aluminum/composite drive shaft was 3.3 kg, which was only 25% of the conventional steel drive shaft. The static torque capability and the fundamental natural frequency were 4320 Nm and 9390 rpm, which exceeded the design requirements.

Acknowledgements

This work has been supported by NRL Project of Korean Government and, in part, by BK21 project.

References

[1] Reimpell J, Stroll H. The automotive chassis: engineering principles. New York: Society of Automotive Engineers; 1996.

[2] Schmelz F, Seherr-Thoss C, Aucktor E. Universal Joints and Driveshafts. New York: Springer-Verlag; 1992.

[3] Cho DH, Lee DG, Choi JH. Manufacturing of one-piece automotive driveshafts with aluminum and composite materials. Compos Struct 1997;38:309–19.

[4] Kim JK, Lee DG, Cho DH. Investigation of adhesively bonded joints for composite propeller shafts. J Compos Mater 2001;35:999–1021.

[5] Mallick PK. Fiber-Reinforced Composites. New York: Marcel Dekker; 1988. p. 2–3.

[6] Chon TC. Analysis of tubular lap joint in torsion. J Compos Mater 1982;16:268–84.

[7] DeGarmo EP, Black JT, Kohser RA. Materials and Processing in Manufacturing. New York: John Wiley and Sons; 1999. p. 966–1033.

[8] Mallick PK, Newman S. Composite Materials Technology. Hanser Publishers; 1990. p. 206–10.

[9] Cho DH, Lee DG. Manufacturing of co-cured aluminum composite shafts with compression during co-curing operation to reduce residual thermal stresses. J Compos Mater 1998;32:1221–41.

[10] Wyrick DA, Adams DF. Residual strength of a carbon/epoxy composite material subjected to repeated impact. J Compos Mater 1988;22(8):749–65.

[11] Springer GS. Environmental Effects on Composite Materials. New York: Technomic Publishing Company; 1981.

[12] Timoshenko SP, Gere JM. Theory of Elastic Stability. New York: McGraw-Hill; 1963. p. 500–9.

[13] Lalanne M, Berthier O, Hagopian JD, Nelson FC. Mechanical Vibration for Engineers. New York: John Wiley and Sons; 1983. p. 102–5.

[14] Choi JH, Lee DG. Torque capacity of co-cured tubular lap joints. J Compos Mater 1997;31(14):1381–96.

[15] Cho DH, Lee DG. Optimum design of co-cured steel-composite tubular single lap joints under axial load. J Adhesion Sci Tech 2000;14(7):939–63.

[16] Gibson RF. Principles of the Composite Material Mechanics. New York: McGraw-Hill; 1994. p. 110–2.

[17] Zou ZR, Gu SR, Vincent L. An investigation of the fretting wear of two aluminum alloys. Tribol Int 1997;30(1):1–7.

[18] Juuma T. Torsional fretting fatigue strength of a shrink-fitted shaft. Wear 1990;231:310–8.

[19] Pilkeym WD. Perterson's Stress Concentration Factors. 2nd ed. New York: John Wiley and Sons; 1997. p. 408–40.